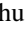



Realizing large out-of-plane magnetic anisotropy in $L1_0$ -FeNi films grown by nitrogen-surfactant epitaxy on Cu(001)

Kaishu Kawaguchi ¹, Toshio Miyamachi,^{1,*} Takushi Iimori,¹ Yuki Takahashi ^{1,2}, Takuma Hattori,¹ Toshihiko Yokoyama,^{3,4} Masato Kotsugi,² and Fumio Komori^{1,†}

¹*Institute for Solid State Physics, The University of Tokyo, Kashiwa, Chiba 277-8581, Japan*

²*Faculty of Industrial Science and Technology, Tokyo University of Science, 6-3-1, Nijjuku, Katsushika, Tokyo 125-8585, Japan*

³*Department of Materials Molecular Science, Institute for Molecular Science, Myodaiji-cho, Okazaki 444-8585, Japan*

⁴*Department of Structural Molecular Science, The Graduate University for Advanced Studies (SOKENDAI), Myodaiji-cho, Okazaki 444-8585, Japan*



(Received 13 November 2019; revised manuscript received 4 April 2020; accepted 7 April 2020; published 6 May 2020)

Rare-metal free ferromagnetic material $L1_0$ FeNi with large uniaxial magnetic anisotropy has attracted much attention for broad use of magnetic materials in various applications. While single-crystal films of $L1_0$ FeNi can be made by layer-by-layer epitaxial growth, magnitude of the uniaxial anisotropy has been lower than expected because of the imperfection of the crystal atomic structure. Here, a nitrogen (N) -surfactant epitaxial growth below 150 K is employed for overcoming interlayer mixing of the atoms at the interface. Ordered $L1_0$ FeNi films are successfully prepared on the Cu(001) substrate precovered by a Ni_2N monolayer. The role of the N surfactant and the absence of the intermixing among Fe and Ni during the deposition and annealing processes were investigated by scanning tunneling microscopy and x-ray photoemission spectroscopy. Element-specific magnetic properties were *in situ* studied by soft-x-ray magnetic circular dichroism (XMCD). The observed Fe hysteresis curve and XMCD of the nitrogen-covered Ni/Fe/Ni trilayer indicate an out-of-plane magnetocrystalline anisotropy large enough for dominating the film shape anisotropy. The N-surfactant epitaxy provides a useful method for fabricating well-ordered magnetic materials without rare metals.

DOI: [10.1103/PhysRevMaterials.4.054403](https://doi.org/10.1103/PhysRevMaterials.4.054403)

I. INTRODUCTION

Critical to the development of magnetic materials for practical use is uniaxial magnetic anisotropy with high magnetic moment, coercivity, and transition temperature [1]. To utilize them widely, such as for magnetic memory devices and electric motors, rare-element free materials are strongly required [2]. Ferromagnetic ultrathin films are particularly desirable for the spintronic applications [3]. One of the excellent candidates of rare-metal free materials is $L1_0$ FeNi with large uniaxial anisotropy energy, K_u , up to 1.3 MJ m^{-3} [4], whereas its single crystal cannot be prepared by conventional macroscopic crystal growth. It has been reported that single crystal $L1_0$ FeNi films can be made by layer-by-layer molecular beam epitaxy (MBE) on Cu(001) and other substrates in a vacuum [5–7]. The maximum K_u so far observed in the epitaxially grown films is 0.7 MJ m^{-3} [6]. The values similar to this were estimated in the cases of $L1_0$ FeNi prepared by denitrogenation [8] and pulsed-laser deposition (PLD) [9]. Thus, the magnetic anisotropy perpendicular to the $L1_0$ FeNi film has not been realized because the in-plane film shape anisotropy is larger than the magnetocrystalline anisotropy. The limitation of the K_u value in the epitaxial films has been attributed to

the following two nonideal processes in the growth: one is an imperfect layer-by-layer mode and the other is interlayer mixing of the atoms at the interface during the growth over 200°C [5,6].

In the present paper, we demonstrate significant improvement of the uniaxial magnetic anisotropy of an $L1_0$ FeNi epitaxial film prepared by combination of surfactant epitaxy [10] of Fe and Ni atomic layers using nitrogen (N) atoms and the deposition on a cooled Cu(001) substrate. The N-surfactant epitaxy, that is, successive and selected segregation of the N atoms to the surface during the alternate Fe and Ni monolayer deposition in the present case, suppresses the mixing between Fe and Ni atoms during the deposition and annealing. It was previously demonstrated on the N-adsorbed Cu(001) substrate that N atoms segregate to the surface during the Co deposition without mixing between the Co and Cu atoms [11]. This is quite in contrast to the mixing during the deposition of magnetic transition metals on the same substrate, which was confirmed by atomically resolved observations using scanning tunneling microscopy (STM) [12,13]. Sharp interface between the atomic layers of the $L1_0$ FeNi film is achieved by the present method. The cooled substrate ensures a monatomic layer growth while the bilayer islands are formed by the deposition above room temperature (RT). Our schema of the N-surfactant growth of the $L1_0$ FeNi thin film on Cu(001) is given in Fig. 1. The top layer is always a nitride atomic layer (iron nitride FeN or nickel nitride NiN)

*toshio.miyamachi@issp.u-tokyo.ac.jp

†komori@issp.u-tokyo.ac.jp

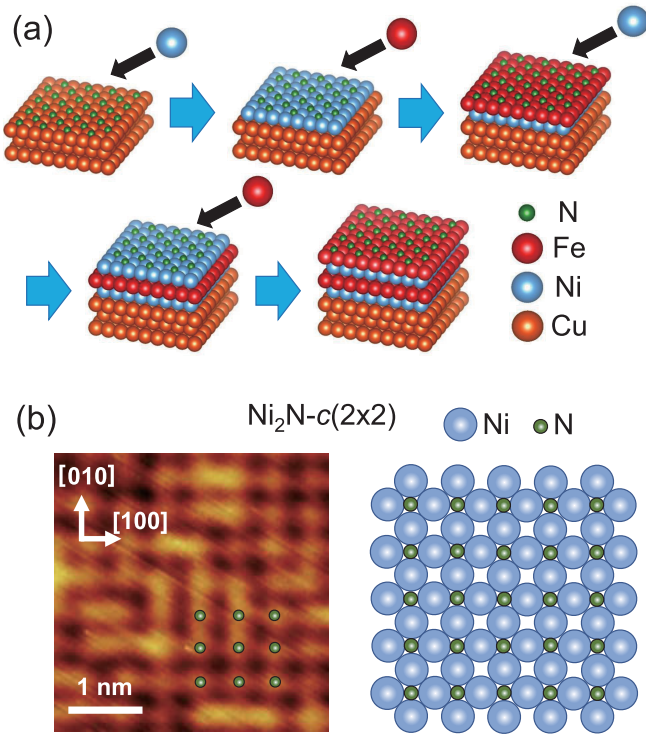


FIG. 1. (a) Schematic model of an FeN/Ni/Fe/Ni film formation process on Cu(001) by surfactant epitaxy using N atoms. (b) STM image of a Ni_2N atomic layer on Cu(001) (left) and its ball model (right).

after deposition of Fe or Ni. For the trilayer FeNi film thus prepared, the Fe hysteresis curve measured using element-specific soft-x-ray magnetic circular dichroism (XMCD) indicates the out-of-plane magnetocrystalline anisotropy is large enough for overcoming the in-plane film shape anisotropy.

II. EXPERIMENT

The $L1_0$ thin films of Ni and Fe were fabricated on the Cu(001) substrate in a UHV ($<2.0 \times 10^{-10}$ Torr) in the following way. First, the Cu(001) surface was cleaned by cycles of Ar^+ sputtering and annealing at 500°C . Next, the substrate at RT was exposed to 500 eV N^+ ions followed by monatomic layer (ML) Ni deposition from a high-purity (99.99%) Ni rod using an electron-bombardment-type evaporator. Here, ML is defined as the atomic density of the Cu(001) surface. Then, a well-ordered Ni_2N atomic layer was made on Cu(001) by annealing at 400°C for 10 min. At this stage, a $c(2 \times 2)$ Ni_2N atomic layer [14] appears on the Cu(001) substrate as the STM image shows in Fig. 1(b). The stoichiometry of the Ni_2N layer was previously confirmed by x-ray photoemission spectroscopy (XPS) in comparison with the N-adsorbed Cu(001) surface [14]. On top of the Ni_2N atomic layer cooled below 150 K, we further deposited monolayer Fe and Ni alternatively from an Fe (99.998%) rod and the Ni rod using the same type evaporators. Before the third Ni and the fourth Fe layer deposition below 150 K, the films were once annealed up to RT for more than 30 min.

The STM topographic images were obtained at RT in a constant current mode using a tungsten tip. The XPS measurements were carried out at RT using a hemispherical electron analyzer and Mg or Al x-ray sources. We used two separated measurement systems for STM and XPS. Each system has a UHV chamber equipped with a low-energy electron diffraction (LEED) optics for preparing the samples, which were transferred to each measurement chamber in UHV through a gate valve. The x-ray absorption spectroscopy (XAS)/XMCD measurements were carried out at BL 4B of UVSOR-III [15] in a total electron yield mode at 8 K using left and right circular polarized light. The circular polarization of the incident x ray was set to 65%. The absorption spectra were recorded in the normal incidence (NI) ($\theta = 0^\circ$) and grazing incidence (GI) ($\theta = 55^\circ$) geometries. Here, we define the incident x-ray angle θ as the angle between the surface normal and the incident x ray. The external magnetic field up to 5 T was applied in parallel or antiparallel to the incident x ray. The XMCD spectrum was obtained by reversing the magnetic field while the photon helicity was fixed to one alignment because of the technical limitation on the frequent switching of the photon helicity. The XMCD intensity is defined as $I_+ - I_-$, where I_+ and I_- denote the absorption intensity at the Fe or Ni $L_{2,3}$ edges with the photon helicity parallel (+) and antiparallel (−) to the external magnetic field. The magnetization curve was obtained by plotting the Fe L_3 absorption peak intensity normalized by the L_2 one with a single photon helicity as a function of magnetic field [16]. The XAS/XMCD measurement system has an UHV sample-preparation chamber with a LEED optics, from where the samples were transferred to the measurement chamber in UHV.

III. RESULTS AND DISCUSSION

A. STM study

A topographic STM image of the surface after deposition of 0.8 ML Fe on the Ni_2N surface is shown in Fig. 2(a). Most of the Fe islands have monoatomic height in contrast to the growth of 2-ML-high Fe islands at RT [17]. The layer-by-layer growth is promoted by reducing the surface diffusion of the Fe atoms on the cooled Ni_2N surface. As indicated in the magnified STM and LEED images shown in Figs. 2(b) and 2(c), however, the island surface was not well ordered while the bare Ni_2N surface kept the $c(2 \times 2)$ structure.

The lattice order of the monolayer Fe islands was systematically studied by LEED after 10 min annealing between 200 and 400°C [16]. The $c(2 \times 2)$ spot becomes sharp with increasing the annealing temperature T_a up to 300°C while the LEED intensity at the $p4gm(2 \times 2)$ spot gradually increases after the annealing over 250°C . The latter suggests the formation of the $p4gm(2 \times 2)$ Fe_2N monoatomic layer on Cu(001) [18], which was confirmed by our STM observations, and is attributed to thermal diffusion of the Ni atoms into the Cu substrate.

For suppressing the Ni diffusion into the substrate Cu, we decreased T_a to 150°C and prolonged the annealing time up to 10 h. Then, a flat and ordered surface was successfully prepared as in Figs. 2(e)–2(g). A magnified STM image

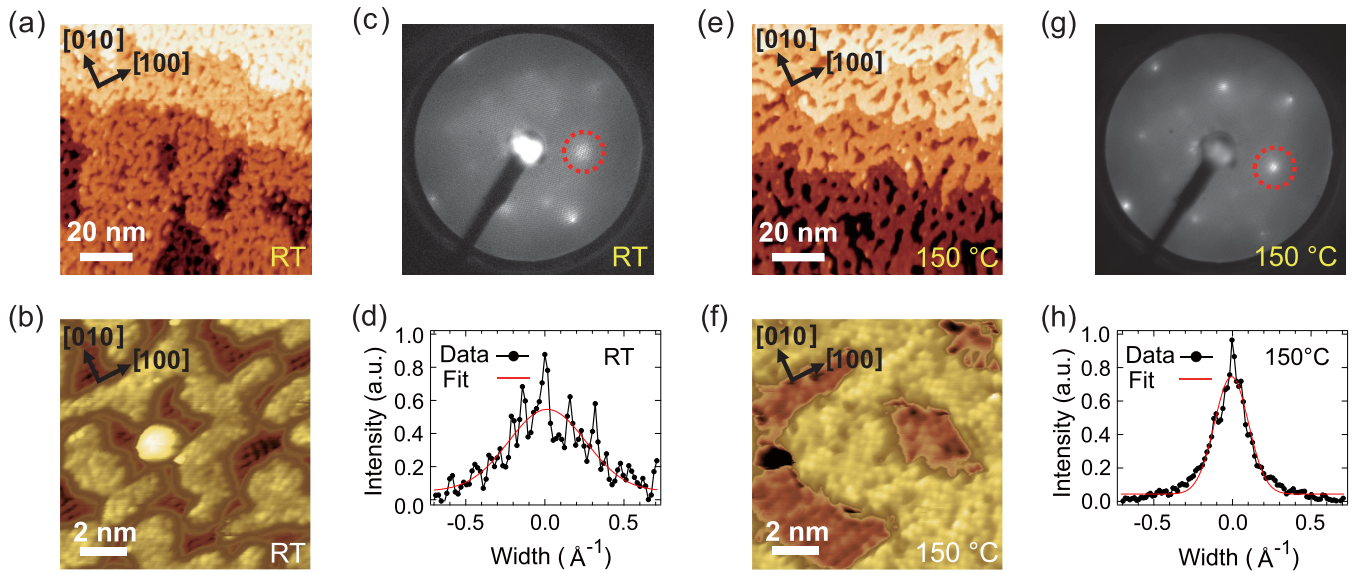


FIG. 2. STM [(a),(b),(e),(f)] and LEED [(c),(g)] images, and profiles of the (1,0) LEED spots [(d),(h)] indicated by the red circles in the corresponding LEED images of a Ni_2N atomic layer after deposition of 0.8-ML Fe on average at 150 K. The Fe deposition amount of 0.8 ML was set for observing the structure of the underlayer Ni_2N . The images were taken at RT before [(a)–(c)] and after [(e)–(g)] 10-h annealing at 150 °C. In (b) and (f), the image contrast is modified nonlinearly to show the surface structures of the overlayer, and the original substrate can be seen clearly. Red curves in (d) and (h) are Gaussian curves fitted to the data with the full widths half maximum 0.7 and 0.3 \AA^{-1} , respectively. The electron energy for LEED was 110 eV.

shown in Fig. 2(f) indicates atomically ordered areas on the surface while the island surface was disordered before the annealing as in Fig. 2(b). The terrace is well connected and the LEED spots become sharp after the 10-h annealing as indicated by the profiles shown in Figs. 2(d) and 2(h). The 10-h annealing at higher than 150 °C should be avoided because the significant diffusion of the Ni atoms into the substrate was confirmed as the increase of the LEED intensity at the $p4gm(2 \times 2)$ spot after the 200 °C annealing [16].

B. XPS study

To confirm the surfactant effect of N and the intermixing among Cu, Ni, and Fe during the annealing processes up to 450 °C for 10 min, XPS signals of these elements were *in situ* measured at RT [16]. The Fe and Ni monatomic layers were alternately deposited on the Ni_2N monolayer at 80 K. The results are summarized in Fig. 3 for the Fe-deposited (bilayer) and both Fe- and Ni-deposited (trilayer) Ni_2N surfaces.

The integrated intensity of the N 1s signal is almost the same for $T_a \leq 300$ °C as that before the Fe deposition as shown in Fig. 3(a). The N atoms are always at the surface as surfactant for $\text{RT} \leq T_a \leq 300$ °C. Thermal desorption of the N atoms can be concluded from the decrease of the N 1s signal for $T_a \geq 350$ °C. The segregation of N atoms above RT was also confirmed by XPS for the NiN/Fe/Ni trilayer and FeN/Ni/Fe/Ni quadruple layer as shown in Fig. 4. It is noted that oxygen cannot be used for the surfactant epitaxy in the present case, because Cu atoms are known to segregate during transition-metal deposition at RT on the oxygen-adsorbed Cu(001) [19,20].

The observed decrease of the Ni $2p_{3/2}$ intensity after the Fe deposition and annealing at RT for the FeN/Ni bilayer in

Fig. 3(b) indicates that the Ni layer is below the Fe layer. The estimated fraction of Ni atoms in the surface FeN layer is less than 10% at RT. This value was obtained using the universal curve of photoelectron escape depth for the observed Ni $2p_{3/2}$ intensity after the Fe deposition. Thermal diffusion of the Ni atoms into the Cu substrate is recognized also from the decrease of Ni $2p_{3/2}$ intensity for $T_a > 300$ °C in Fig. 3(b), and the mixing of Fe atoms with Ni and Cu from the decrease of the Fe $2p_{3/2}$ intensity for $T_a \geq 400$ °C in Fig. 3(c). In the case of the NiN/Fe/Ni trilayer, the Fe $2p_{3/2}$ intensity in the grazing emission increased as in Fig. 3(d). This confirms the intermixing between subsurface Fe atoms and surface Ni atoms above 350 °C.

C. Magnetic properties

In this section, we focus on the magnetic properties of the trilayer and quadruple-layer films prepared after 10-h annealing at the stage of the FeN/Ni bilayer, where the surface is flat and ordered, and suitable for the further Ni and Fe growth. We show the results of Fe XAS and XMCD for the NiN/Fe/Ni trilayer after RT annealing in Fig. 5(a). They were recorded at Fe $L_{2,3}$ absorption edges in the NI and GI geometries. The value of Fe XMCD is an order of magnitude larger than that of Ni $L_{2,3}$ XMCD, and thus the Fe monolayer dominates the magnetism of the film. It is noted that no XMCD signal was detected in the Ni_2N monolayer without Fe overlayer at 8 K in 5 T.

Figures 5(b) and 5(c) display the Fe element-specific magnetization curves of the NiN/Fe/Ni trilayer and FeN/Ni/Fe/Ni quadruple layer. These were obtained from the field-dependent Fe XAS data in the NI and GI geometries. The magnetization curves of the trilayer exhibits excellent

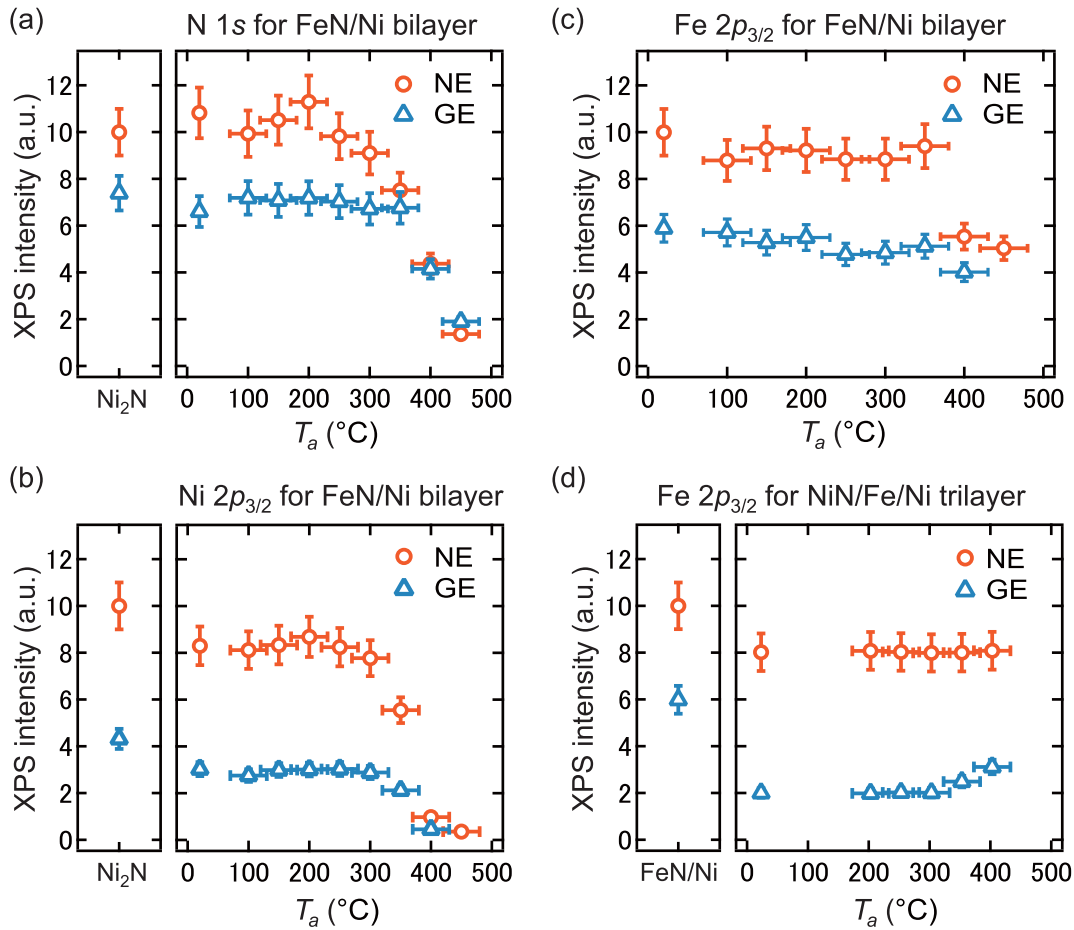


FIG. 3. (a)–(c) Integrated intensity of N 1s XPS (a), Ni 2p_{3/2} XPS (b), and Fe 2p_{3/2} XPS (c) from a FeN/Ni bilayer for normal (NE) and grazing (60° off from the surface normal, GE) emission as a function of the annealing temperature T_a . (d) Integrated intensity of Fe 2p_{3/2} XPS from a NiN/Fe/Ni trilayer for NE and GE as a function of T_a . The N and Ni XPS intensity at RT from the Ni₂N surface for NE is set to be 10 in (a) and (b), respectively. In (c), the Fe XPS intensity at RT for NE is set to be 10, and in (d), that before the Ni deposition.

ferromagnetic behaviors, and the out-of-plane magnetization curve has a slightly steeper slope around the origin (zero magnetic field) than that in the GI geometry. The result indicates

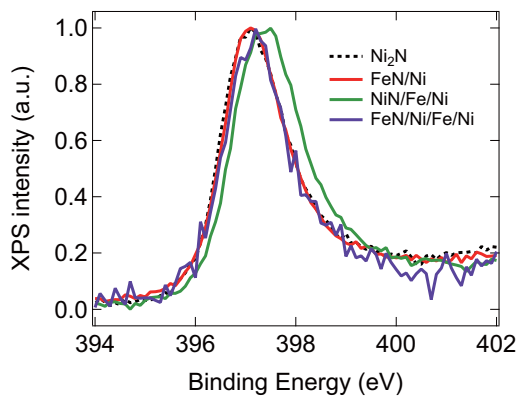


FIG. 4. N 1s XPS data in the normal emission geometry for the Ni₂N monatomic layer, FeN/Ni bilayer, NiN/Fe/Ni trilayer, and FeN/Ni/Fe/Ni quadruple layer after RT annealing. No reduction of the intensity was observed by successive Fe and Ni deposition at 80 K.

that the out-of-plane magnetic anisotropy is realized against the in-plane film shape anisotropy in the trilayer. In contrast, for the quadruple layer, the magnetization curve in the GI geometry has a steeper slope around the origin than that in the NI geometry. The out-of-plane magnetocrystalline anisotropy of the quadruple layer is insufficient for dominating the film shape anisotropy as in all the previous results of the MBE-grown $L1_0$ FeNi films. In the quadruple layer, there are two different kinds of Fe layers: one is monolayer Fe between the Ni monolayers and the other is monolayer FeN at the surface. The latter could weaken the out-of-plane anisotropy because the Fe₂N monolayer on Cu(001) has an in-plane magnetic anisotropy [21,22].

It is noted that the importance of the interface magnetic anisotropy was pointed out previously in the studies of the related system, Fe-covered pure Ni films on Cu(001) [23–27]. Out-of-plane magnetic anisotropy of the Ni films has been reported in a thickness range between 7–10 ML and 40–70 ML [28–30]. The Fe overlayer modifies the critical thickness of the anisotropy change from in-plane to out-of-plane with changing the Fe thickness. This change is attributed to the interface magnetic anisotropy. The present results on the $L1_0$ FeNi films indicate that the interface magnetic anisotropy can

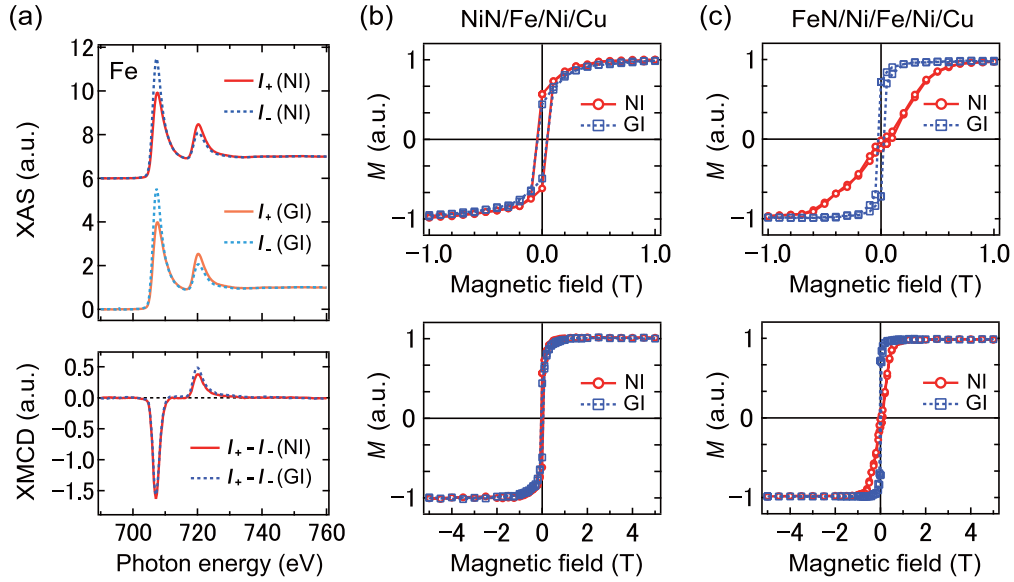


FIG. 5. (a) Fe L -edge XAS (upper) and XMCD (lower) spectrum of the NiN/Fe/Ni trilayer after RT annealing for the NI and GI geometries. The XAS intensity was measured with the photon helicity parallel (I_+) and antiparallel (I_-) to the external magnetic field. (b),(c) Narrow- (upper) and wide- (lower) range Fe magnetization (M) curves of the NiN/Fe/Ni trilayer (b) and FeN/Ni/Fe/Ni quadruple layer (c). In the GI geometry, the magnetic field direction is 55° off from the surface normal to the [100] direction of the Cu(001) substrate.

be affected by the atomic-scale disorder and intermixing in the system.

Here we estimate values of K_u in the present sample by using the saturation magnetization of the MBE-grown $L1_0$ FeNi film as follows. The difference of the magnetic energy E_{NI} and E_{GI} between the NI and GI geometries can be obtained from the following equation with the magnetization (M - H) curves,

$$E_{\text{NI}} - E_{\text{GI}} = \mu_0 \int H dM_{\text{NI}} - \mu_0 \int H dM_{\text{GI}}, \quad (1)$$

where M_{NI} and M_{GI} are the magnetization in the NI and GI geometries, and μ_0 the vacuum permeability. The estimated values of the energy difference using the M - H curves shown in Figs. 5(b) and 5(c) are -0.1 ± 0.02 and 0.30 ± 0.02 MJ m^{-3} for the NiN/Fe/Ni trilayer and the FeN/Ni/Fe/Ni quadruple layer, respectively. The field-direction dependence of the magnetic energy E_θ is phenomenologically given [21] as

$$E_\theta = \left(\frac{\mu_0 M_s^2}{2} - K_u \right) \cos^2(\theta) - \mu_0 M_s H \cos(\theta_M - \theta), \quad (2)$$

where θ is the angle between the surface normal and the direction of the magnetic field H , M_s the saturation magnetization, and θ_M the polar angle of the magnetization. When we use the saturation magnetization of the MBE-grown $L1_0$ FeNi film [6] and assume $\theta_M = \theta$ for $\theta = 0$ and 55° , K_u is estimated from Eq. (2) as 1.0 ± 0.02 and 0.45 ± 0.02 MJ m^{-3} for the NiN/Fe/Ni trilayer and the FeN/Ni/Fe/Ni quadruple layer, respectively. The value of K_u for the trilayer is overestimated because the magnetic moment of the Ni layers is smaller than that of the MBE-grown $L1_0$ FeNi film [31]; the bottom Ni layer is adjacent to the nonmagnetic Cu substrate, and the top Ni layer is not of pure Ni, but nickel nitride. The monatomic

Ni layer on both Cu(001) [32] and Ni₄N [33] is known to have magnetic moments smaller than metallic pure Ni. We can expect the increases of M_s and thus the value of K_u by increasing the thickness of the $L1_0$ film.

By applying the XMCD sum rules [34,35] to the Fe XMCD data in 5 T for the trilayer, effective spin magnetic moment $m_{\text{spin}}^{\text{eff}} (=m_s + 7m_T)$, which dominantly contributes to the amplitude of the magnetization, and orbital magnetic moment m_{orb} are quantitatively evaluated. Here, m_s is the spin magnetic moment and m_T is the magnetic dipole moment. We used the average number of Fe $3d$ holes 3.22, which was estimated as in literature [21]. The value of $m_{\text{spin}}^{\text{eff}}$ thus obtained is $1.7 \pm 0.1 \mu_B$, which is larger than that ($1.6 \mu_B$) of a 4-ML $L1_0$ FeNi grown on a Ni(001) film by MBE [36] and smaller than that ($2.0 \mu_B$) of a thick $L1_0$ FeNi film grown on a Cu(001) film by MBE [31]. This suggests the saturation magnetization of the trilayer is smaller than that of the thick $L1_0$ FeNi film [6]. We can expect a further increase of $m_{\text{spin}}^{\text{eff}}$ by repeating the N-surfactant growth of the alternate Ni and Fe layers; in the case of a few atomic layers, the nitrogen-adsorbed surface layer can weaken the magnetism of the inner $L1_0$ FeNi layers with out-of-plane anisotropy as well as the paramagnetic Cu substrate [32]. Using the XMCD sum rules, we can also evaluate out-of-plane and in-plane orbital magnetization, m_{orb}^\perp and m_{orb}^\parallel , from the experimental data and discuss the magnetic anisotropy [37,38]. The evaluated values of m_{orb}^\perp and m_{orb}^\parallel are 0.31 ± 0.05 and $0.16 \pm 0.07 \mu_B$ for the trilayer, and are consistent with the out-of-plane anisotropy.

IV. CONCLUSION

We have investigated the structural and magnetic properties of a-few-atomic-layer $L1_0$ FeNi prepared by a layer-by-layer

N-surfactant epitaxy. The $L1_0$ FeNi epitaxial growth is realized on the monolayer- Ni_2N -covered Cu substrate cooled below 150 K. The role of the N surfactant and the absence of the intermixing among Fe, Ni, and Cu during the deposition and post-annealing even for 10 h at 150 °C are confirmed by STM, LEED, and XPS. Using the element-specific magnetic properties studied by XMCD, we have demonstrated that the out-of-plane anisotropy is large enough for overcoming the film shape anisotropy for the trilayer film. The N-surfactant epitaxy opens a way to fabricate well-ordered element-strategic magnetic material such as a $L1_0$ FeNi film. Designing of novel functional materials could be accelerated by multilateral characterization using microscopic, macroscopic, and spectroscopic analyses.

ACKNOWLEDGMENTS

The authors thank T. Gozłinski, T. Koiyaya, O. Ishiyama, and E. Nakamura for collaboration on the XAS/XMCD experiments. They also thank I. Matsuda, M. Mizuguchi, and K. Takanashi for fruitful discussion on our results. This work was partly supported by JSPS KAKENHI for Young Scientists (A), Grant No. 16H05963; for Scientific Research (B), Grants No. 16H03873, No. 18K01146, and No. 19H02595; Shimadzu Science Foundation; and Nanotechnology Platform Program (Molecule and Material Synthesis) of the Ministry of Education, Culture, Sports, Science and Technology (MEXT). T.H. was supported by the Program for Leading Graduate Schools (MERIT) and the Grant-in-Aid for JSPS Research Fellow.

-
- [1] D. Li, Y. Li, D. Pan, Z. Zhang, and C.-J. Choi, Prospect and status of iron-based rare-earth-free permanent magnetic materials, *J. Magn. Magn. Mater.* **469**, 535 (2019).
- [2] J. Cui, M. Kramer, L. Zhou, F. Liu, A. Gabay, G. Hadjipanayis, B. Balasubramanian, and D. Sellmyer, Current progress and future challenges in rare-earth-free permanent magnets, *Acta Mater.* **158**, 118 (2018).
- [3] G. Scheunert, O. Heinonen, R. Hardeman, A. Lapicki, M. Gubbins, and R. M. Bowman, A review of high magnetic moment thin films for microscale and nanotechnology applications, *Appl. Phys. Rev.* **3**, 011301 (2016).
- [4] L. Neel, D. Dautreppe, J. Laugier, J. Pauleve, and R. Pauthenet, Magnetic properties of iron-nickel single crystal ordered by neutron bombardment, *J. Appl. Phys.* **35**, 873 (1964).
- [5] T. Shima, M. Okamura, S. Mitani, and K. Takanashi, Structure and magnetic properties for $L1_0$ -ordered FeNi films prepared by alternate monatomic layer deposition, *J. Magn. Magn. Mater.* **310**, 2213 (2007).
- [6] T. Kojima, M. Ogiwara, M. Mizuguchi, M. Kotsugi, T. Koganezawa, T. Ohtsuki, T.-Y. Tashiro, and K. Takanashi, Fe-Ni composition dependence of magnetic anisotropy in artificially fabricated $L1_0$ -ordered FeNi films, *J. Phys.: Condens. Matter* **26**, 064207 (2014).
- [7] K. Takanashi, M. Mizuguchi, T. Kojima, and T. Tashiro, Fabrication and characterization of $L1_0$ -ordered FeNi thin films, *J. Phys. D* **50**, 483002 (2017).
- [8] S. Goto, H. Kura, E. Watanabe, Y. Hayashi, H. Yanagihara, Y. Shimada, M. Mizuguchi, K. Takanashi, and E. Kita, Synthesis of single-phase $L1_0$ -FeNi magnet powder by nitrogen insertion and topotactic extraction, *Sci. Rep.* **7**, 13216 (2017).
- [9] M. Saito, H. Ito, Y. Suzuki, M. Mizuguchi, T. Koganezawa, T. Miyamachi, F. Komori, K. Takanashi, and M. Kotsugi, Fabrication of $L1_0$ -FeNi by pulsed-laser deposition, *Appl. Phys. Lett.* **114**, 072404 (2019).
- [10] W. F. Egelhoff and D. A. Steigewald, The role of adsorbed gases in metal on metal epitaxy, *J. Vac. Sci. Technol. A* **7**, 2167 (1989).
- [11] D. Sekiba, S. Doi, K. Nakatsuji, and F. Komori, Effects of strain field in nitrogen-mediated Co film growth on Cu(001): Segregation and electronic structure change, *Surf. Sci.* **590**, 138 (2005).
- [12] F. Nouvertné, U. May, M. Bammig, A. Rampe, U. Korte, G. Güntherodt, R. Pentcheva, and M. Scheffler, Atomic exchange processes and bimodal initial growth of Co/Cu(001), *Phys. Rev. B* **60**, 14382 (1999).
- [13] H. L. Meyerheim, R. Popescu, D. Sander, J. Kirschner, O. Robach, and S. Ferrer, Layer relaxation and intermixing in Fe/Cu(001) studied by surface x-ray diffraction, *Phys. Rev. B* **71**, 035409 (2005).
- [14] Y. Hashimoto, K. Nakatsuji, T. Iimori, and F. Komori, Atomic and nanostructures of monolayer $c(2 \times 2)\text{NiN}$ on Cu(001), *Surf. Sci.* **604**, 451 (2010).
- [15] T. Nakagawa, Y. Takagi, Y. Matsumoto, and T. Yokoyama, Enhancements of spin and orbital magnetic moments of submonolayer Co on Cu(001) studied by X-ray magnetic circular dichroism using superconducting magnet and liquid He cryostat, *Jpn. J. Appl. Phys.* **47**, 2132 (2008).
- [16] S. Nakashima, T. Miyamachi, Y. Tatetsu, Y. Takahashi, Y. Takagi, Y. Gohda, T. Yokoyama, and F. Komori, Dynamic interface formation in magnetic thin film heterostructures, *Adv. Funct. Mater.* **29**, 1804594 (2019).
- [17] See Supplemental Material at <http://link.aps.org/supplemental/10.1103/PhysRevMaterials.4.054403> for additional STM and LEED images, and XPS data.
- [18] Y. Takahashi, T. Miyamachi, K. Ienaga, N. Kawamura, A. Ernst, and F. Komori, Orbital Selectivity in Scanning Tunneling Microscopy: Distance-Dependent Tunneling Process Observed in Iron Nitride, *Phys. Rev. Lett.* **116**, 056802 (2016).
- [19] X. D. Liu, T. Iimori, K. Nakatsuji, and F. Komori, Invasive growth of Co on $(\sqrt{2} \times 2\sqrt{2})R45^\circ$ reconstructed O/Cu(001), *Appl. Phys. Lett.* **88**, 133102 (2006).
- [20] H. L. Meyerheim, J.-M. Tonnerre, L. Sandratskii, H. C. N. Tolentino, M. Przybylski, Y. Gabi, F. Yildiz, X. L. Fu, E. Bontempi, S. Grenier, and J. Kirschner, New Model for Magnetism in Ultrathin fcc Fe on Cu(001), *Phys. Rev. Lett.* **103**, 267202 (2009).
- [21] Y. Takagi, K. Isami, I. Yamamoto, T. Nakagawa, and T. Yokoyama, Structure and magnetic properties of iron nitride thin films on Cu(001), *Phys. Rev. B* **81**, 035422 (2010).
- [22] Y. Takahashi, T. Miyamachi, S. Nakashima, N. Kawamura, Y. Takagi, M. Uozumi, V. N. Antonov, T. Yokoyama, A. Ernst,

- and F. Komori, Thickness-dependent electronic and magnetic properties of γ' -Fe₄N atomic layers on Cu(001), *Phys. Rev. B* **95**, 224417 (2017).
- [23] W. L. O'Brien and B. P. Tonner, Room-temperature magnetic phases of Fe on fcc Co(001) and Ni(001), *Phys. Rev. B* **52**, 15332 (1995).
- [24] B. Schirmer and M. Wuttig, Antiferromagnetic coupling in fcc Fe overlayers on Ni/Cu(100), *Phys. Rev. B* **60**, 12945 (1999).
- [25] X. Liu and M. Wuttig, Magnetic properties of Fe/Ni bilayers on Cu(100), *Phys. Rev. B* **64**, 104408 (2001).
- [26] R. Ramchal, A. K. Schmid, M. Farle, and H. Poppa, Spiral-like continuous spin-reorientation transition of Fe/Ni bilayers on Cu(100), *Phys. Rev. B* **69**, 214401 (2004).
- [27] R. Thamankar, S. Bhagwat, and F. Schumann, Effect of sub-monolayer coverage of Fe and Mn films on the magnetization direction of Ni/Cu(100), *J. Magn. Magn. Mater.* **281**, 206 (2004).
- [28] F. Huang, M. T. Kief, G. J. Mankey, and R. F. Willis, Magnetism in the few-monolayers limit: A surface magneto-optic Kerr-effect study of the magnetic behavior of ultrathin films of Co, Ni, and Co-Ni alloys on Cu(100) and Cu(111), *Phys. Rev. B* **49**, 3962 (1994).
- [29] W. L. O'Brien and B. P. Tonner, Transition to the perpendicular easy axis of magnetization in Ni ultrathin films found by x-ray magnetic circular dichroism, *Phys. Rev. B* **49**, 15370 (1994).
- [30] B. Schulz and K. Baberschke, Crossover from in-plane to perpendicular magnetization in ultrathin Ni/Cu(001) films, *Phys. Rev. B* **50**, 13467 (1994).
- [31] M. Kotsugi, M. Mizuguchi, S. Sekiya, M. Mizumaki, T. Kojima, T. Nakamura, H. Osawa, K. Kodama, T. Ohtsuki, T. Ohkochi, K. Takanashi, and Y. Watanabe, Origin of strong magnetic anisotropy in L1₀-FeNi probed by angular-dependent magnetic circular dichroism, *J. Magn. Magn. Mater.* **326**, 235 (2013).
- [32] A. Ernst, M. Lueders, W. Temmerman, Z. Szotek, and G. van der Laan, Theoretical study of magnetic layers of nickel on copper; dead or alive? *J. Phys.: Condens. Matter* **12**, 5599 (2000).
- [33] Y. Imai, Y. Takahashi, and T. Kumagai, Relations of electronic energies and magnetic moments of tetra-3d metal (Mn, Fe, Co and Ni) nitrides calculated using a plane-wave basis method, *J. Magn. Magn. Mater.* **322**, 2665 (2010).
- [34] B. T. Thole, P. Carra, F. Sette, and G. van der Laan, X-Ray Circular Dichroism as a Probe of Orbital Magnetization, *Phys. Rev. Lett.* **68**, 1943 (1992).
- [35] C. T. Chen, Y. U. Idzerda, H.-J. Lin, N. V. Smith, G. Meigs, E. Chaban, G. H. Ho, E. Pellegrin, and F. Sette, Experimental Confirmation of the X-Ray Magnetic Circular Dichroism Sum Rules for Iron and Cobalt, *Phys. Rev. Lett.* **75**, 152 (1995).
- [36] M. Sakamaki and K. Amemiya, Element specific magnetic anisotropy energy of alternately layered FeNi thin films, *Appl. Phys. Express* **4**, 073002 (2011).
- [37] P. Bruno, Tight-binding approach to the orbital magnetic moment and magnetocrystalline anisotropy of transition-metal monolayers, *Phys. Rev. B* **39**, 865 (1989).
- [38] G. van der Laan, Microscopic origin of magnetocrystalline anisotropy in transition metal thin films, *J. Phys.: Condens. Matter* **10**, 3239 (1998).